

Tunable Multiresonant Microcavity Exciton-Polaritons in Colloidal Quantum Wells

Nhung Vu Cam,[○] Md Abdur Rahman,[○] Syed Akhil, Emek Goksu Durmusoglu, Thi Thu Ha Do, Pedro Ludwig Hernandez-Martinez, Corentin Dabard, Deepshikha Arora, Siam Uddin, Golnoush Zamiri, Hao Wang, Son Tung Ha, N. Asger Mortensen, Hilmi Volkan Demir,* and Joel K.W. Yang*



Cite This: *Nano Lett.* 2025, 25, 6109–6116



Read Online

ACCESS |



Metrics & More



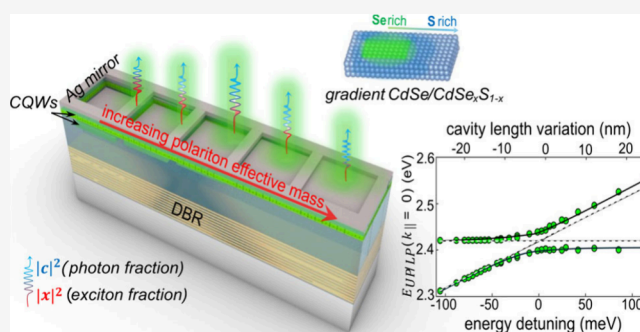
Article Recommendations



Supporting Information

ABSTRACT: Optical microcavities are widely used to confine photons for exciton-polariton formation. However, their compact design often imposes limitations on spatial freedom, particularly in controlling the cavity length with the nanometer precision required for effective coupling with excitons. Existing methods for tuning resonances by integrating cavities with dynamic structures often lack sufficient resolution or a complex operation. Here, we introduce a multiresonant microcavity array that provides a full spectral selection of cavity resonances with a sub-5 nm cavity length variation. We employed this platform to investigate room-temperature polariton formation using gradient core-crown colloidal quantum wells that host highly stable excitons. The strong coupling system exhibits longevity of Rabi oscillations with a quality factor of $Q_R = 3.3$ and a large Rabi splitting exceeding twice the thermal losses. Notably, we achieved control of the polariton mixed properties across the cavity arrays on a single substrate. This platform is promising for the development of on-chip polaritonic devices.

KEYWORDS: exciton-polaritons, tunable, colloidal quantum wells, on-chip devices



Optical microcavities provide a versatile platform for strong coupling between excitons and photons, resulting in the formation of hybrid states known as microcavity polaritons. They were first observed experimentally by Weisbuch et al. in 1992,¹ using a Fabry-Pérot (FP) cavity composed of two distributed Bragg reflectors (DBRs) to trap photons in between. To date, this configuration remains the most widely used for polaritonic studies, enabling the demonstrations of room-temperature Bose-Einstein condensation,^{2,3} quantum fluids,^{4,5} and low-threshold polariton lasing.^{6–8} A key advantage of such structures is their ease of fabrication, currently using only thin-film deposition techniques, which renders them well-suited for wafer-scale production. However, a long-standing challenge persists in precisely adjusting the cavity length to control the detuning between cavity resonance and exciton energy. This precision should fall within the narrow exciton transition line width, which can be as small as 10 nm.⁹ The difficulty primarily arises during the thin-film deposition process, which includes techniques such as physical vapor deposition and chemical vapor deposition of dielectric layers or spin coating of the excitonic material. Inhomogeneous films or cavities with thickness variations are frequently observed, especially when colloidal materials are considered.^{10–12} In previous studies, the identification of a suitable cavity mode was achieved by

scanning of a laser beam across the cavity surface, aided by random variations across the sample.^{10,12,13} Furthermore, the closed design of these microcavities presents a limitation in tunability, which is a drawback compared to open-surface cavities.

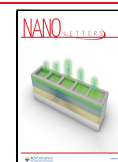
To enhance the flexibility of microcavities, mounting mirrors on nanopositioners offers fine-tuning with nm precision but is complex for chip-scale polaritonic applications.^{14,15} Liquid crystal (LQ)-integrated microcavities also provide tunability but are limited to the microscale by thick cavity lengths.¹⁶ Recently, ultralow-loss phase change materials (PCMs)-based DBR has been employed for continuous tuning;¹⁷ however, the tuning range is coarse, as it involves shifting the entire photonic bandgap of the DBR. On the other hand, tunable coupling can also be achieved by adjusting the excitonic properties; for example, temperature variation is the common approach.¹⁸ However, this method causes a change in exciton

Received: January 2, 2025

Revised: March 7, 2025

Accepted: March 10, 2025

Published: March 13, 2025



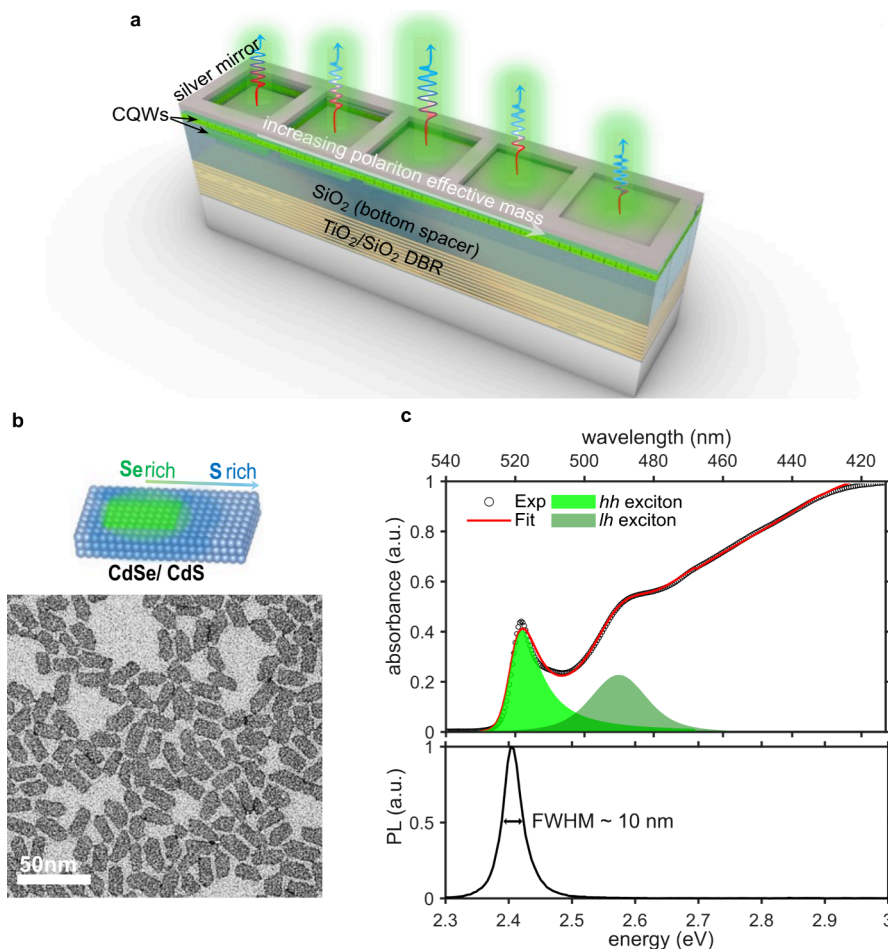


Figure 1. A multiresonant microcavity polariton device. (a) Schematic of the multiresonant Tamm-plasmon microcavity array consisting of DBR/silver mirrors embedding a thin film of CQWs and dielectric spacers. The cavity length varies, resulting in variation of the exciton/photon fraction of polariton emission across the array. (b) Schematic illustration of the gradient C/C CdSe/CdS CQWs, along with a TEM image. (c) Absorbance-photoluminescence (PL) spectra of the CQWs thin film fitted with the particle-in-a-box quantum model (red line). Green filled curves are the fitted absorbance of hh (heavy hole) and lh (light hole) excitons, respectively.

binding energy. Therefore, a long-standing challenge remains to develop a microcavity platform that offers precise, on-demand tunability for polariton applications that can be integrated into on-chip devices and remains stable and compatible with various excitonic materials.

Here, we introduce multiresonant microcavity arrays fabricated using a binary lithography and reflow (BLR) method to address the current limitations of compact cavity structures with superior tunability, stability, and integration. The most striking feature of this process is its ability to integrate multiple microcavities on a single substrate with an ultrasmall step cavity length variation of sub-5 nm, across a controlled broad range, all with a single-step lithography process. This approach allows for self-consistent measurements from one cavity to another as the undesired influences from other variables are eliminated. Unlike MEMS or piezoelectric-based tuning,^{14,19} which have limited operational lifetimes, our *static* tuning approach is inherently more stable and less complex. Moreover, our BLR fabrication method allows multiple resonant states to be integrated on the same substrate, unlike open-cavity systems, which require sequential tuning. These advantages make our platform highly scalable and ideal for large-scale production.

We employed these microcavity arrays for room-temperature strong coupling with gradient core-crown (C/C) CdSe/CdSe_xS_{1-x} colloidal quantum wells (CQWs). We reported these CQWs recently and demonstrated their photophysical and excitonic properties.²⁰ Polaritons and lasing in CQWs have previously been demonstrated using various cavity systems, including plasmonic nanoholes,²¹ nanoparticle lattices,²² metallic films,²³ and FP microcavities.²⁴ However, these studies have primarily focused on core-only CQWs that often suffer from nonradiative exciton recombination due to the inefficient passivation of surface trap states. In this work, we used our gradient C/C CQWs as they offer better optical stability while preserving high exciton binding energy, making them more suitable for polariton studies.²⁰ Using the microcavity array, we achieved simultaneous energy detuning between cavity photons and excitons over a broad range, up to three times the exciton line width, while remaining within the same cavity mode order. A complete anticrossing of polariton emission with varying cavity resonance is observed, unambiguously confirming strong coupling. Additionally, by controlling the detuning energy, we can modulate the exciton/photon ratio, the Hopfield coefficients, in the normal direction across the cavity array, thereby simultaneously adjusting the polariton effective mass. These advancements hold significant promise

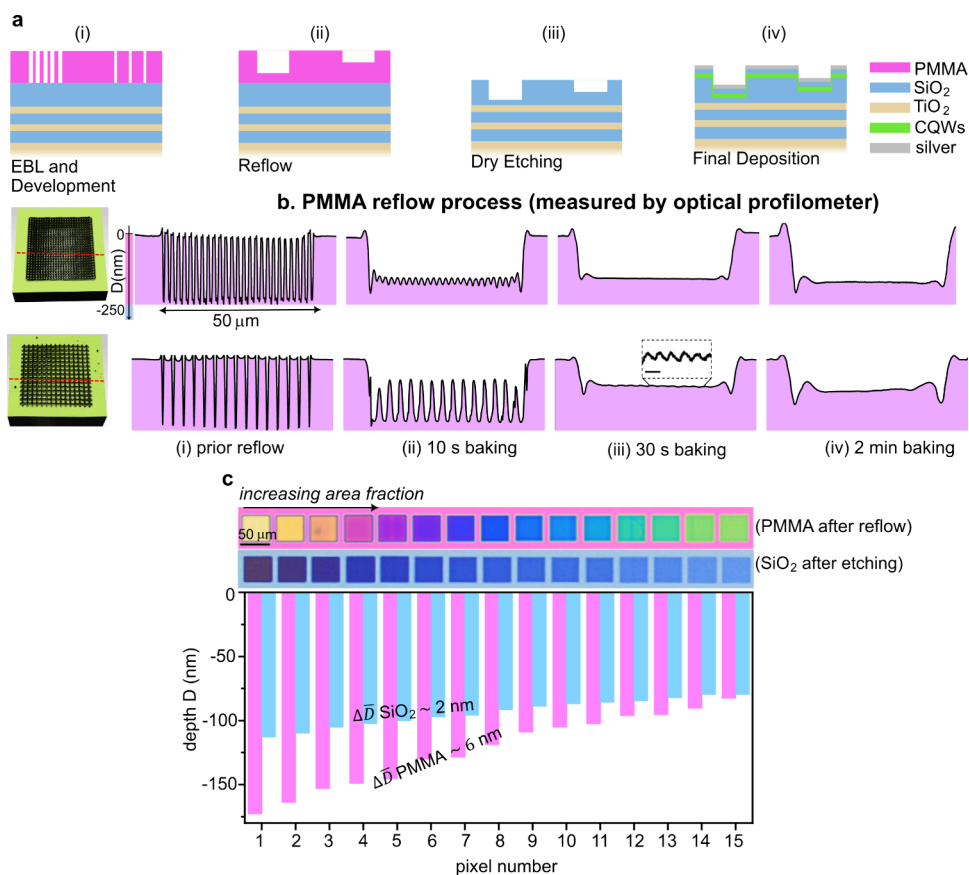


Figure 2. Fabrication process for microcavity arrays with cavity length variations. (a) Fabrication process flow. (b) Cross-sectional profile of PMMA pixels at different reflow stages measured using a 3D optical profilometer. Top panel: 30% area fraction. Bottom panel: 60% area fraction. Inset (b)-iii: zoomed-in surface profile of PMMA (scale bar: 20 nm) (c) Optical microscopy (OM) images of 15 pixels after PMMA reflow and after pattern transfer via etching into SiO₂, along with a plot showing the corresponding depth variation (D) measured for each pixel at each stage using ellipsometry. $\Delta\bar{D}$ represents the average step depth.

for the development of on-chip polariton devices. It is worth noting that the device and fabrication technique proposed here can also be applied to other photonic systems using high-quality factor FP cavities such as tunable vertical-cavity surface-emitting lasers (VCSELs) or high-purity color filters.

A schematic illustration of the multiresonant microcavity array is shown in Figure 1a. The array is designed to create multiple distinct resonant cavities by controllably varying the thickness of the bottom dielectric spacer while keeping the thicknesses of the layers above constant. Each square pixelated cavity has a lateral size of 50 μm with a 10 μm separation between neighboring cavities. Afterward, a thin film of CQWs is spin-coated onto the array, encapsulated by dielectric spacers, and embedded within Tamm plasmon microstructures,¹² composed of DBR and silver mirrors. This approach allows for precise control of the cavity resonance on a single substrate, requiring only a single lithographic step.

In CQWs, the conventional type-I core/crown heterostructure consists of a CdSe core and a CdS crown, where the CdS crown passivates the periphery of the CdSe core, enhancing the photoluminescence quantum yield (PLQY).^{25,26} In this study, we choose gradient CdSe/CdSe_xS_{1-x} C/C CQWs as the emitter layer. The gradient interface between core and crown layers was achieved through the sequential growth of the CdSe core and CdSe_xS_{1-x} crown layers in a one-pot reaction,²⁰ rather than the separate synthesis of CdSe core and CdS crown growth as previously

reported.²⁷ Detailed synthesis procedures are provided in the Supporting Information. As a result of the alloyed interface, the gradient C/C CQWs exhibited enhanced PLQY of 92%, while the conventional C/C CQWs exhibited lower PLQY of 78%.²⁰ Transmission electron microscopy (TEM) images of the synthesized gradient C/C CdSe/CdSe_xS_{1-x} CQWs are shown in Figure 1b. TEM images show the quasi-rectangular shape of the CQWs, with uniform lateral dimensions of approximately 13 \times 22 nm and a thickness of 1.4 nm, equivalent to 4.5 monolayers (MLs) (Figure S2). Energy-dispersive X-ray spectroscopy (EDS) line scans on individual CQWs²⁰ demonstrated the compositional gradient and smooth transition from the CdSe core to the CdS crown in our previous study. Compared to conventional C/C heterostructures with sharp interfaces, the gradient C/C architecture exhibits improved photostability (Figure S3) and thermal stability (Figure S4) with enhanced PLQY. At the same time, it maintains a high binding energy, making it suitable for exciton-polariton strong coupling. To compare lasing stability, we deposited both C/C and gradient C/C CQWs on glass substrates with identical thicknesses and pumped them using a femtosecond laser (Movie S1, Movie S2). Our results show that, above a certain pump power threshold, amplified spontaneous emission (ASE) peaks appeared in both samples. However, while the ASE almost immediately disappeared in the C/C CQWs, it persisted throughout the measurement duration (up to several minutes) and remained stable in the

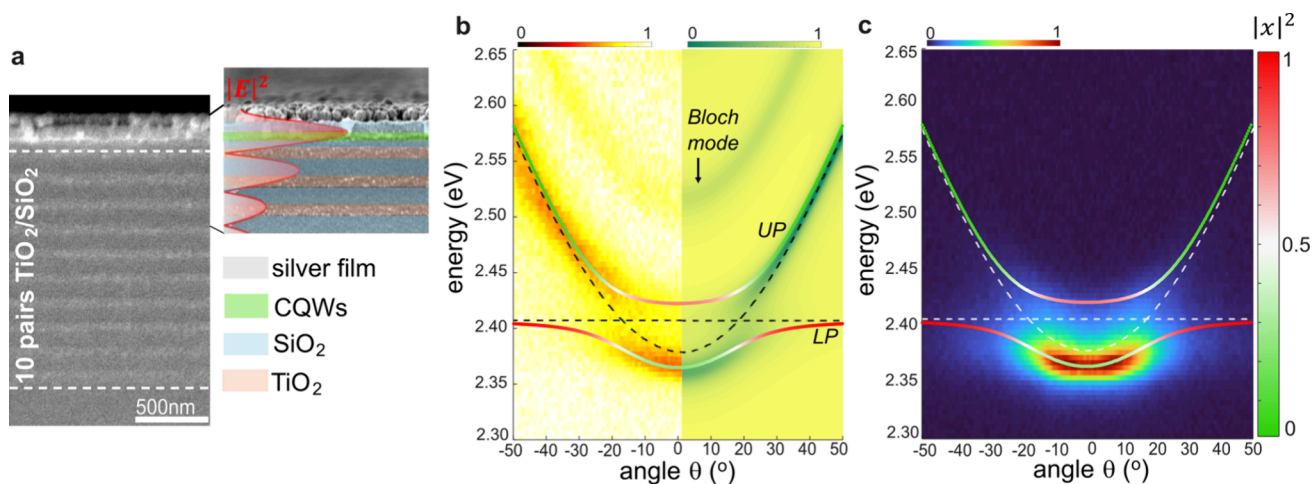


Figure 3. Room-temperature exciton-polariton formation in the planar Tamm plasmon cavity with a gradient of C/C CQWs. (a) Cross-sectional SEM image of the planar Tamm cavity device. Right panel: simulated electric field intensity $|E|^2$ at the cavity resonance. The thicknesses of the top SiO_2 spacer, CQWs, and bottom SiO_2 spacer are 50, 40, and 42 nm, respectively. (b) The left/right panels show the measured/calculated angle-resolved reflectivity dispersion, respectively. (c) Angle-resolved PL dispersion. In (b-c), the dashed lines correspond to bare cavity photon and hh exciton energies. The solid lines indicate calculated upper polariton (UP) and lower polariton (LP) branches with the color representing the excitonic fraction $|x|^2$ of each branch.

gradient C/C CQWs. This is direct proof demonstrating the superior stability of the gradient C/C architecture.

Figure 1c shows the normalized absorption and PL spectra of the CQW thin film. The absorption spectrum features a heavy-hole (*hh*) exciton transition at 2.42 eV, with a broader band at higher energies attributed to light-hole (*lh*) transitions and alloying within the CQW crown.²⁸ This type of particle presents a quasi-type-I band alignment, leading to a concentration of the excitons in the CdSe core. Thus, the corresponding PL spectrum exhibits an emission at 2.4 eV with a small Stokes shift of 20 meV corresponding to the band edge emission in CdSe 4.5 MLs. To extract the exciton binding energy, the absorption spectra were produced theoretically with well-resolved excitonic bands, based on the particle-in-a-box model for the quantum confinement of the excitons.²⁹ For simplification, only the *hh* and *lh* transitions have been considered. The alloy contribution in the core-crown gradient interface has been accounted using a Gaussian-like function to average its influence on the absorption features. A value of 210 meV is found for this structure, which is lower than that for the core and core-crown cases (Figure S5). This could be explained by reduced Coulomb interactions between the two charge carriers induced by the larger delocalization of both holes and electrons inside the gradient C/C CQWs in comparison to conventional C/C CQWs (Figure S6). However, the important features for strong coupling, the narrow line width of the *hh* exciton band of ~ 10 nm and the high exciton binding energy of around 200 meV, are preserved.

To alter the cavity length, we employ the binary electron-beam lithography process to control the filling area of the patterned poly(methyl methacrylate) (PMMA) resist, followed by a heat reflow process to level the resist surface (Figure 2a, i-ii). Throughout the entire patterning process, the exposure dose was maintained at a constant value. As demonstrated in our recent work,³⁰ the remaining PMMA after an optimized reflow heat treatment exhibits a thickness that is linearly dependent with the area fraction of patterned pixels. Here, we extend the approach by a pattern transfer step into an inorganic SiO_2 layer. The profile of the reflowed PMMA layer

of varying thickness is transferred onto the underlying SiO_2 surface via dry etching, creating similar patterns on this dielectric surface but with an important reduction in profile depth by ~ 3 times due to the corresponding higher etch rate of PMMA to SiO_2 (Figure 2a, iii). These variations in the dielectric film will ultimately determine the cavity length variation in the microcavity array. To complete the cavity, the CQWs, top SiO_2 spacer, and silver mirror are successively deposited (Figure 2a, iv). The key advantage of BLR is that it allows the simultaneous deposition and processing of these layers for multiple cavities. This property ensures a controlled experiment with mutually self-consistent cavities, where the only variable is the cavity length. Furthermore, the BLR process requires only a single lithographic step, eliminating the need for separate processing steps for each cavity.

In Figure 2b, we closely examine the PMMA reflow process using a 3D optical profilometer (Profilom3D) to measure the surface profiles of the sample at various stages of the reflow. We studied two patterned pixels of binary square pillars with area fractions of 30% and 60%, respectively. After 10 s of baking, the PMMA pillars began melting uniformly and filling the voids between them. Leveling was observed in the high-density pattern after heating 30 s, while the low-density pattern continued reflowing. The continuous flat film began forming on this pixel after 2 min of heating. Although the sidewalls were not straight due to the reflow process, the central region became flat (Figure 2b, iv). As expected, the reflowed low-density pattern was twice as thick as the high-density pattern, demonstrating the linear proportionality between the thickness and the area fraction.

Finally, an array of 15 pixels with a varying area fraction was fabricated, and the OM images after PMMA reflow and after etching into SiO_2 are shown in Figure 2c. We used the ellipsometry to measure the thickness of PMMA and SiO_2 in each pixel, and using independently obtained information on the dielectric functions we then deduced the depth D , as shown in the graph of Figure 2c. The average step depth ΔD , defined as the depth difference of the first and last pixels divided by the total number of pixels, was reduced by a factor

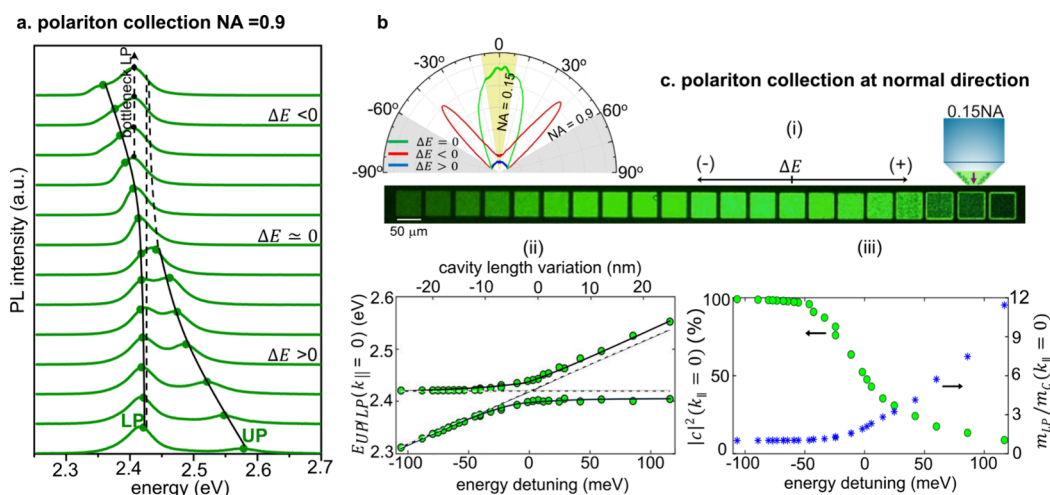


Figure 4. Exciton-polariton formation in the multiresonant microcavity array. (a) PL spectra of polariton emission measured for individual pixels using a 0.9 NA objective. The straight dashed line corresponds to the hh-exciton energy of C/C CQWs. Solid curves guide the peak energies of the LP and UP branches. The UP branch is merely detected for $\Delta E < 0$ (dashed curve). Dots highlight the peaks of LP, UP, and bottleneck LP. (b) Polariton emission diagram of three selected cavity pixels with zero, negative, and positive detuning. (c) Polariton emission characterized at a normal direction: (i) PL image of the cavity array collected with a 0.15 NA objective, (ii) UP and LP energies $E_{UP/LP}$ at normal incidence ($k_{||} = 0$) plotted as a function of the energy detuning and corresponding cavity length variation, and (iii) photon fraction $|c|^2$ and the LP effective mass m_{LP}/m_C (normalized by photon effective mass m_C).

of 3 down to ~ 2 nm after etching. This reduction is proportional to the etching rate ratio of SiO_2 and PMMA.

We first realize the room-temperature strong coupling between the gradient C/C CQWs and a single planar Tamm plasmon cavity. A cross-sectional SEM image of the fabricated cavity is shown in Figure 3a. The DBR consists of 10 pairs of $\text{TiO}_2/\text{SiO}_2$, supporting nearly unity reflectivity ($R \sim 99.9\%$) with a broad photonic stopband of 500–700 nm. Measuring the reflectance at normal incidence of the Tamm plasmon cavity, we deduced an experimental quality factor of $Q = 115$ (Figure S7). Here, the C/C CQWs layer was placed around the maxima of the electric field to ensure optimal coupling to the cavity mode (Figure 3a).

Figure 3b,c shows the reflectivity and PL dispersions measured using angle-resolved spectroscopy. For PL dispersion, the characterization is performed under weak, nonresonant excitation using a 405 nm continuous-wave laser. As can be seen in Figure 3b, both upper polariton (UP) and lower polariton (LP) branches are visible in the reflectivity map, with a distinct anticrossing at angles $\sim 20^\circ$. However, the UP branch is barely discernible in the PL dispersion, as shown in Figure 3c. This is mainly due to the high density of states of the polaritons at the excitonic reservoir near the inflection points, which causes relaxation pathways to bypass the UP branch.³¹ The dispersion of polariton branches closely matches the theoretical eigenenergies obtained from the coupled oscillator model³² (see Supporting Information). Additionally, by using the transfer matrix method and treating the exciton as a classical Lorentz oscillator³¹ (Figure S1), we can map out the reflectivity dispersion as shown in Figure 3b.

From the reflectivity dispersion, we extract the Rabi splitting to be $\hbar\Omega_R = 50$ meV, and the uncoupled photon-exciton detuning is $\Delta E = -30$ meV. To confirm the coupling regime, we use Rabi quality factor Q_R , which quantifies the number of resolvable Rabi oscillations in time-resolved spectroscopy.^{33,34} It is defined as

$$Q_R = \frac{\sqrt{(2\hbar\Omega_R)^2 - (\Gamma_{hh} - \Gamma_C)^2}}{\Gamma_{hh} + \Gamma_C} \quad (1)$$

where $\Gamma_{hh} = 10$ meV and $\Gamma_C = 20$ meV are the line widths of bare hh excitons and cavity, respectively. The Γ_{hh} is obtained by fitting the absorbance spectrum to the particle-in-a-box quantum model. Note that $Q_R > 1$ corresponds to the common strong-coupling criteria, that the Rabi splitting is greater than average line widths $\hbar\Omega_R > (\Gamma_{hh} + \Gamma_C)/2$; however, Q_R can be used to compare different strong coupling systems as it is normalized to the intrinsic properties of the system. We estimate that $Q_R = 3.3$, which unambiguously confirms the strong coupling regime. This value is greater than the Q_R reported for CQWs in the other systems^{21,23,24} and is comparable to that of cavity-based surface lattice resonance (SLR),²² which can support polariton lasing. The large Rabi splitting and longevity of the Rabi oscillations demonstrate that the gradient C/C CQWs could be a robust excitonic material at room temperature. The excitonic and photonic fractions of LP, defined by Hopfield coefficients³² $|x|^2$ and $|c|^2$ (see Supporting Information), are indicated by the color gradient along the polariton dispersion lines in Figure 3b,c. As the result of negative detuning ($\Delta E < 0$), the LP exhibits a photonic-dominated character at near-zero angles and becomes an exactly half-photon, half-exciton state at the anticrossing point. It is worth noting that the effective mass and lifetime of polaritons are determined by the Hopfield coefficients, which, in turn, depend on the detuning ΔE . Thus, the ability to control energy levels of microcavities is crucial for manipulating the mixed photon-exciton properties of polaritons.

The design and fabrication of the cavity array are detailed in Figures 1 and 2. Figure 4a shows the PL spectra measured by stitching the laser excitation beam across each pixel. The polariton emission was collected over a wide angular range by using a 0.9 NA microscope objective. The anticrossing of the LP and UP branches is clearly observed due to variations in ΔE . As previously mentioned, the UP-peak positions could not be identified for negative detuning. We now present the

polariton formation of the CQWs in a multiresonant microcavity array, where the cavity resonance can be precisely tuned on-demand across the exciton energy range. We show it as a dash line that asymptote to the exciton energy in Figure 4a. We observe that near zero detuning ($\Delta E \approx 0$), the UP and LP and peaks are not well-resolved in the PL spectra. To further confirm strong coupling, we performed angle-resolved PL measurements for these detunings, as shown in Figure S8, where the polariton branches are clearly resolved. Additionally, when $\Delta E < -50$ meV, new peaks emerge below the exciton energy ($E_x = 2.42$ eV), dominating the LP resonance and remaining unchanged with detuning, as indicated by the dashed arrow. The corresponding angle-resolved PL spectrum (Figure S8) reveals that polaritons tend to accumulate at higher angles near the inflection points rather than relax down to the LP valley. This phenomenon is attributed to bottleneck polaritons, which represent a significant challenge that hinders polariton condensation in similar systems.^{35,36} Leveling up the detuning flattens the LP dispersion, thereby mitigating the bottleneck issue.³² Therefore, modulating the cavity level is important for facilitating polariton relaxation.

The subsequent section of this study focuses on the polariton emission of the microcavity array in the forward direction. Figure 4c,i shows the PL image of the microcavity array, captured by using a 0.15 NA objective. The polariton emission is the brightest at zero detuning and decreases as the detuning shifts toward either negative or positive values. This is because, for negative detuning, polaritons predominantly occupy large angles (as shown in the emission diagram in Figure 4b), while, for positive detuning, the emission of the UP branch is largely absorbed by other energy bands of CQWs.

The UP and LP energies at angle $\theta = 0^\circ$ were determined by fitting the angle-resolved PL dispersion of each pixelated cavity with the theoretical eigenenergies (see Supporting Information), and these energies were plotted against the cavity length variation and its corresponding energy detuning (Figure 4c, (ii)). By combining three different pattern designs for BLR in the microcavity array (Figure S9), we can vary the cavity length by approximately ± 30 nm with an average step of 2 nm, with the cavity length at $\Delta E = 0$ eV taken as the reference point. This enables a broad spectral tunability of cavity photon energy exceeding 100 meV, which is twice the Rabi splitting. Finally, by adjusting the cavity length, we can finely tune the exciton-photon ratio of polaritons, thereby enabling precise control over the polaritonic properties within our cavity system. As shown in Figure 4c, iii, the photonic fraction $|d|^2$ gradually decreases along the microcavity arrays as ΔE shifts from negative to positive values, leading to a simultaneous increase in the LP effective mass m_{LP} . Since the exciton effective mass m_x^{hh} is much larger than the photon effective mass m_C (in the order of 10^{-5} times), we can approximate $m_{LP}/m_C = 1/|d|^2$.

In conclusion, we have observed clear exciton-polariton formation at room temperature in the gradient C/C CQWs coupled with Tamm-plasmon microcavities. The use of multiresonant microcavity arrays has enabled the measurement of a complete anticrossing of polariton energies with varying energy detuning, thereby allowing the continuous variation of the effective mass of the polariton on a single substrate. This approach enhances design flexibility and provides better control of exciton-photon coupling in optical microcavities. In future work, reducing the pixel sizes and spacing between neighboring pixels should be investigated. This tunable cavity

thickness, enabling precise energy level control, paves the way for the realization of polariton condensation in a cascaded energy lattice.

■ ASSOCIATED CONTENT

Supporting Information

The Supporting Information is available free of charge at <https://pubs.acs.org/doi/10.1021/acs.nanolett.5c00015>.

Microcavity fabrication; CQWs synthesis and characterization; angle-resolved spectroscopy; coupled oscillator model; Lorentz oscillator model; size distribution of gradient C/C CQWs; thermal and photo stability comparison between the gradient and conventional C/C CQWs; the experimental absorption spectra fitted by the particle-in-a-box model; calculation of the distribution of charge density within the gradient and conventional C/C CQWs; angle-resolved reflectivity spectra of the bare cavity at normal incidence $\theta = 0^\circ$; polariton detuning in the multiresonant microcavity array; three types of patterns were used to fabricate the multiresonant microcavity array (PDF)

Movie S1, amplified spontaneous emission of the C/C CQWs (MP4)

Movie S2, amplified spontaneous emission of the gradient C/C CQWs (MP4)

■ AUTHOR INFORMATION

Corresponding Authors

Hilmi Volkan Demir – LUMINOUS! Center of Excellence for Semiconductor Lighting and Displays, The Photonics Institute, School of Electrical and Electronic Engineering, School of Physical and Mathematical Sciences, School of Materials Science and Engineering, Nanyang Technological University, Singapore 639798, Singapore; UNAM-Institute of Materials Science and Nanotechnology and National Nanotechnology Research Center, Department of Electrical and Electronics Engineering, Department of Physics, Bilkent University, Bilkent, Ankara 06800, Turkey; orcid.org/0000-0003-1793-112X; Email: hvdemir@ntu.edu.sg

Joel K.W. Yang – Engineering Product Development, Singapore University of Technology and Design, Singapore 487372, Singapore; POLIMA-Center for Polariton-driven Light-Matter Interactions and Danish Institute for Advanced Study, University of Southern Denmark, DK-5230 Odense M, Denmark; orcid.org/0000-0003-3301-1040; Email: joel_yang@sutd.edu.sg

Authors

Nhung Vu Cam – Engineering Product Development, Singapore University of Technology and Design, Singapore 487372, Singapore; orcid.org/0000-0003-0885-5698

Md Abdur Rahman – Engineering Product Development, Singapore University of Technology and Design, Singapore 487372, Singapore; orcid.org/0000-0003-3199-9251

Syed Akhil – LUMINOUS! Center of Excellence for Semiconductor Lighting and Displays, The Photonics Institute, School of Electrical and Electronic Engineering, School of Physical and Mathematical Sciences, School of Materials Science and Engineering, Nanyang Technological University, Singapore 639798, Singapore

Emek Goksu Durmusoglu – LUMINOUS! Center of Excellence for Semiconductor Lighting and Displays, The

Photonics Institute, School of Electrical and Electronic Engineering, School of Physical and Mathematical Sciences, School of Materials Science and Engineering, Nanyang Technological University, Singapore 639798, Singapore; orcid.org/0000-0001-6840-8342

Thi Thu Ha Do – Institute of Materials Research and Engineering (IMRE), Agency for Science, Technology and Research (A*STAR), Singapore 138634, Republic of Singapore

Pedro Ludwig Hernandez-Martinez – LUMINOUS! Center of Excellence for Semiconductor Lighting and Displays, The Photonics Institute, School of Electrical and Electronic Engineering, School of Physical and Mathematical Sciences, School of Materials Science and Engineering, Nanyang Technological University, Singapore 639798, Singapore; orcid.org/0000-0001-6158-0430

Corentin Dabard – LUMINOUS! Center of Excellence for Semiconductor Lighting and Displays, The Photonics Institute, School of Electrical and Electronic Engineering, School of Physical and Mathematical Sciences, School of Materials Science and Engineering, Nanyang Technological University, Singapore 639798, Singapore

Deepshikha Arora – Engineering Product Development, Singapore University of Technology and Design, Singapore 487372, Singapore; orcid.org/0000-0003-0572-342X

Siam Uddin – Engineering Product Development, Singapore University of Technology and Design, Singapore 487372, Singapore

Golnoush Zamiri – Engineering Product Development, Singapore University of Technology and Design, Singapore 487372, Singapore

Hao Wang – School of Instrumentation and Optoelectronic Engineering, Beihang University, Beijing 100191, China; Hangzhou International Innovation Institute, Beihang University, Hangzhou 311115, China; orcid.org/0000-0001-5388-6691

Son Tung Ha – Institute of Materials Research and Engineering (IMRE), Agency for Science, Technology and Research (A*STAR), Singapore 138634, Republic of Singapore; orcid.org/0000-0002-5475-8365

N. Asger Mortensen – POLIMA-Center for Polariton-driven Light-Matter Interactions and Danish Institute for Advanced Study, University of Southern Denmark, DK-5230 Odense M, Denmark; orcid.org/0000-0001-7936-6264

Complete contact information is available at: <https://pubs.acs.org/10.1021/acs.nanolett.5c00015>

Author Contributions

[○](N.V.C., M.A.R.) These authors contributed equally to this work. N.C.V. and M.A.R. initiated the study and contributed equally to this work. J.K.W.Y. and H.V.D. guided the work. E.G.D. and S.A. designed and synthesized CQWs specifically for this work and their conducted optical characterizations. C.D. conducted TEM measurements of CQWs and analyzed TEM data. E.G.D. and N.C.V. developed NPL film deposition on DBR. M.A.R. and N.C.V. fabricated the cavity. G.Z. performed the cross-sectional SEM measurements. S.U. created schematics. P.L.H.M. fitted the CQWs absorption spectra. N.C.V. carried out angle-resolved measurements with assistance from T.T.H.D. and S.T.H. and conducted numerical simulations and theoretical calculations. N.C.V. and M.A.R. performed data analysis and wrote the manuscript with input

from all coauthors. The initial manuscript was written by N.C.V. and M.A.R. and then reviewed and revised by N.A.M., H.V.D., and J.K.W.Y. with the assistance of all authors.

Notes

The authors declare no competing financial interest.

ACKNOWLEDGMENTS

The authors gratefully acknowledge funding support from Singapore MTC-Programmatic Grant No. M21J9b0085. J.K.W.Y. and H.W. acknowledge Singapore University of Technology and Design for the Kickstarter Initiative (SKI) project SKI_2021_04_12. H.V.D. gratefully acknowledge additional support from TUBA-Turkish Academy of Sciences. The Center for Polariton-driven Light-Matter Interactions (POLIMA) is sponsored by the Danish National Research Foundation (Project No.~DNRF165). J.K.W.Y. acknowledges support from the guest professor program of the Otto Mønsted Foundation (Grant No.~23-12-1947).

REFERENCES

- (1) Weisbuch, C.; Nishioka, M.; Ishikawa, A.; Arakawa, Y. Observation of the coupled exciton-photon mode splitting in a semiconductor quantum microcavity. *Phys. Rev. Lett.* **1992**, *69*, 3314.
- (2) Kasprzak, J.; et al. Bose–Einstein condensation of exciton polaritons. *Nature* **2006**, *443*, 409–414.
- (3) Su, R.; et al. Room temperature long-range coherent exciton polariton condensate flow in lead halide perovskites. *Science Advances* **2018**, *4*, No. eaau0244.
- (4) Amo, A.; et al. Superfluidity of polaritons in semiconductor microcavities. *Nat. Phys.* **2009**, *5*, 805–810.
- (5) Peng, K.; et al. Room-temperature polariton quantum fluids in halide perovskites. *Nat. Commun.* **2022**, *13*, 7388.
- (6) Schneider, C.; et al. An electrically pumped polariton laser. *Nature* **2013**, *497*, 348–352.
- (7) Su, R.; et al. Room-temperature polariton lasing in all-inorganic perovskite nanoplatelets. *Nano Lett.* **2017**, *17*, 3982–3988.
- (8) Dusel, M.; et al. Room-temperature topological polariton laser in an organic lattice. *Nano Lett.* **2021**, *21*, 6398–6405.
- (9) Bellessa, J.; et al. Materials for excitons–polaritons: Exploiting the diversity of semiconductors. *MRS Bull.* **2024**, *49*, 932.
- (10) Bouteyre, P.; et al. Room-temperature cavity polaritons with 3D hybrid perovskite: toward large-surface polaritonic devices. *ACS Photonics* **2019**, *6*, 1804–1811.
- (11) Yen, M. C.; et al. Tamm-Plasmon Exciton-Polaritons in Single-Monolayered CsPbBr₃ Quantum Dots at Room Temperature. *Advanced Optical Materials* **2023**, *11*, No. 2202326.
- (12) Symonds, C.; et al. Confined Tamm plasmon lasers. *Nano Lett.* **2013**, *13*, 3179–3184.
- (13) Goblot, V. *Polariton quantum fluids in one-dimensional synthetic lattices: localization, propagation and interactions*; Ph.D. Dissertation, Université Paris Saclay (COMUE), 2019.
- (14) Lackner, L.; et al. Tunable exciton-polaritons emerging from WS₂ monolayer excitons in a photonic lattice at room temperature. *Nat. Commun.* **2021**, *12*, 4933.
- (15) Dufferwiel, S.; et al. Exciton–polaritons in van der Waals heterostructures embedded in tunable microcavities. *Nat. Commun.* **2015**, *6*, 8579.
- (16) Cheng, H.-C.; Kuo, C.-Y.; Hung, Y.-J.; Chen, K.-P.; Jeng, S.-C. Liquid-crystal active Tamm-plasmon devices. *Physical Review Applied* **2018**, *9*, No. 064034.
- (17) Sreekanth, K. V.; et al. Tunable Tamm plasmon cavity as a scalable biosensing platform for surface enhanced resonance Raman spectroscopy. *Nat. Commun.* **2023**, *14*, 7085.
- (18) Liu, X.; et al. Control of coherently coupled exciton polaritons in monolayer tungsten disulphide. *Phys. Rev. Lett.* **2017**, *119*, No. 027403.

- (19) Meng, C.; et al. Dynamic piezoelectric MEMS-based optical metasurfaces. *Science Advances* **2021**, *7*, No. eabg5639.
- (20) Liang, X.; et al. Near-unity emitting, widely tailorable, and stable exciton concentrators built from doubly gradient 2D semiconductor nanoplatelets. *ACS Nano* **2023**, *17*, 19981–19992.
- (21) Winkler, J. M.; et al. Room-temperature strong coupling of CdSe nanoplatelets and plasmonic hole arrays. *Nano Lett.* **2019**, *19*, 108–115.
- (22) Freire-Fernández, F.; et al. Room-Temperature Polariton Lasing from CdSe core-only Nanoplatelets. *ACS Nano* **2024**, *18*, 15177–15184.
- (23) Shlesinger, I.; et al. Strong coupling of nanoplatelets and surface plasmons on a gold surface. *ACS Photonics* **2019**, *6*, 2643–2648.
- (24) Flatten, L. C.; et al. Strong exciton–photon coupling with colloidal nanoplatelets in an open microcavity. *Nano Lett.* **2016**, *16*, 7137–7141.
- (25) Sharma, M.; Delikanli, S.; Demir, H. V. Two-dimensional CdSe-based nanoplatelets: their heterostructures, doping, photo-physical properties, and applications. *Proceedings of the IEEE* **2020**, *108*, 655–675.
- (26) Rodà, C.; et al. Colloidal CdSe/CdS Core/Crown nanoplatelets for efficient blue light emission and optical amplification. *Nano Lett.* **2023**, *23*, 3224–3230.
- (27) Schlosser, A.; Graf, R. T.; Bigall, N. C. CdS crown growth on CdSe nanoplatelets: core shape matters. *Nanoscale Advances* **2020**, *2*, 4604–4614.
- (28) Antanovich, A.; et al. CdSe x S1–x Alloyed Nanoplatelets with Continuously Tunable Blue-Green Emission. *Chem. Mater.* **2022**, *34*, 10361–10372.
- (29) Failla, M.; et al. Observation of the quantized motion of excitons in CdSe nanoplatelets. *Phys. Rev. B* **2020**, *102*, No. 195405.
- (30) Rahman, M. A. Scaling up multispectral color filters with binary lithography and reflow (BLR). *Nanophotonics* **2024**, *13*, 3671.
- (31) Bouteyre, P. *Lasers à pérovskites hybrides halogénées en microcavité*; Ph.D. Dissertation, Université Paris Saclay (COMUE), 2019.
- (32) Deng, H.; Haug, H.; Yamamoto, Y. Exciton-polariton bose-einstein condensation. *Reviews of modern physics* **2010**, *82*, 1489–1537.
- (33) Todisco, F.; et al. Magnetic and electric Mie-exciton polaritons in silicon nanodisks. *Nanophotonics* **2020**, *9*, 803–814.
- (34) Tserkezis, C.; et al. Gain-compensated cavities for the dynamic control of light-matter interactions. *Phys. Rev. A* **2023**, *107*, No. 043707.
- (35) Lai, Y.-Y.; Lan, Y.-P.; Lu, T.-C. Strong light–matter interaction in ZnO microcavities. *Light: Science & Applications* **2013**, *2*, e76.
- (36) Laitz, M.; et al. Uncovering temperature-dependent exciton-polariton relaxation mechanisms in hybrid organic-inorganic perovskites. *Nat. Commun.* **2023**, *14*, 2426.